Computational Study of Band-Crossing Reactions

Alain Matta, Omar M. Knio, Roger G. Ghanem, Chua-Hua Chen, Juan G. Santiago, Bert Debusschere, and Habib N. Najm

***Abstract*—A numerical study of band-crossing reactions is conducted using a quasi-one-dimensional (1-D) computational model that accounts for species bulk advection, electromigration velocities, diffusion, and chemical reaction. The model is used to simulate chemical reactions between two initially distinct sample zones, referred to as "bands," that cross each other due to differences in electromigration velocities. The reaction is described in terms of a single step, reversible mechanism involving two reactants and one product. A parametric study is first conducted of the behavior of the species profiles, and results are interpreted in terms of the Damköhler number and of the ratios of the electromigration velocities of the reactant and product. Computed results are then used to explore the possibility of extracting forward and backward reaction rates based on time resolved observation of integral moments of species concentrations. In particular, it is shown that in the case of fast reactions, robust estimates can be obtained for high forward rates, but that small reverse rates may not be accurately observed. [934]**

***Index Terms*—Binding kinetics, electrochemical processes, electropheretic band crossing, microfluidics, on-chip analysis.**

I. Introduction

MICROFLUIDIC devices have been successfully applied to the analysis of chemical and biological systems. These systems provide many advantages over the conventional biochemical lab analysis, including improved speed and reproducibility, greatly reduced reagent consumption and fabrication cost [1]. Microfluidic devices have in particular been used to quantify a variety of physical parameters [2], including measurements of molecular diffusion coefficients [3], enzyme reaction kinetics [4], [5], and fluid viscosity [6]. Other applications include immunoassays [7]–[9], DNA analysis [10], cell manipulation [11], and capillary electrophoresis [12].

One important class of microfluidic applications concerns kinetic measurements, which provide concise rate expressions that can be used to predict yield, optimize designs, and to provide insight into relevant molecular processes. For example, Hadd *et al.* [4] describe on-chip enzyme assay of beta-galactosidase [4]. Their work clearly showed that the utility of these devices can be extended from the concept of only performing separations to the idea of integrating a complete analysis system. Reagent mixing and transport were accurately controlled by electrokinetic means. Enzyme reaction kinetics were obtained by altering the substrate concentration and measuring the product concentration. Similarly, Chiem *et al.* [8] demonstrated an integrated immunoreactor with electrophoretic separation for serum theophylline determination. In this work, all operations required by the immunoassay like mixing, incubation, separation and detection were automated on the chip.

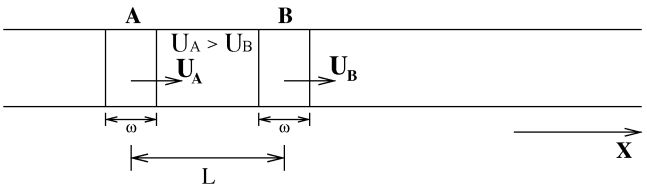

Fig. 1. Schematic illustration of band-crossing reactions, showing the initial structure of reactant bands A and B.

An important challenge in the design of high throughput microfluidic systems concerns the relatively low diffusion rates of many species of interest, particularly macromolecules. Specifically, since characteristic lengthscales are small, the flow is laminar and mixing is generally diffusion-limited, requiring large times for substantial progress of chemical reactions. Consequently, various efforts have been directed at enhancing mixing rates in microfluid devices [13], [15]. Multilamina and splitting techniques are common examples of mixer designs. Mixing induced by lateral transport [13], [14] and electrokinetic instability [15] have also been recently reported.

One attractive alternative to diffusion-controlled reaction is electrophoretically mediated microanalysis (EMMA) [16], [17], which we also refer to as the on-chip electrophoretic band-crossing system [18]. As schematically illustrated in Fig. 1, the setup consists of the simultaneous introduction of two reactive species having different electrophoretic mobilities into a microchannel. The flow is then driven electrokinetically so that the species with the higher electromigration velocity will cross and eventually overtake the one having slower electromigration velocity. Thus, the mixing times are controlled by differences in electromigration velocities, and this distinguishes the present technique from approaches based on fluid stirring, where mixing times are diffusion limited. Since the reactant bands have small width and the electromigration-limited mixing rates are high, this enables rapid observations of fast reactions. The band crossing technique is particularly useful in situations where the fluorescent signal strength of a reaction

Manuscript received September 22, 2002; revised October 1, 2003. This work was supported by the Defense Advanced Research Projects Agency (DARPA) and Air Force Research Laboratory, Air Force Materiel Command, USAF, under agreement F30602-00-2-0612. The U.S. government is authorized to reproduce and distribute reprints for Governmental purposes notwithstanding any copyright annotation thereon. Computations were performed at the National Center for Supercomputer Applications. Subject Editor A. J. Ricco.

A. Matta, O. M. Knio, and R. G. Ghanem are with the Department of Mechanical Engineering, The Johns Hopkins University Baltimore, MD 21218 USA (e-mail: knio@jhu.edu).

C.-H. Chen and J. G. Santiago are with Stanford University Stanford, CA 94305 USA.

B. Debusschere and H. N. Najm are with Sandia National Laboratories, Livermore, CA 94550 USA.

Digital Object Identifier 10.1109/JMEMS.2004.825315

product is low, and a substantial amount of reactants is consequently required for a successful experiment. This in contrast rapid mixing schemes which rely on thin lamination of reactant streams in order to minimize diffusion times [19].

Mathematical [17], [20], [21] and computational [22], [23] models describing the behavior of the EMMA experiments are now well established. The present work builds on prior results by 1) conducting a systematic analysis on the role of various operating parameters such as electromigration velocities, reaction rates and initial concentrations, 2) exploiting the results to establish essential trends and to express these trends in terms of a reduced set of dimensionless parameters, and 3) applying the computations to explore the possibility of extracting kinetic rate constants based on measurements of species concentration profiles. As outlined in Section II, we rely on a quasi-one-dimensional (1-D) model that accounts for species advection and electromigration, reaction and diffusion. Brief dimensional arguments are then introduced in Section III in order to characterize specific flow conditions. Section IV highlights selected results from a detailed parametric study of the effects of reaction rates, differences in electromigration velocities and initial concentrations. An analysis of extraction rate methodologies on basis of integral moments of concentration profiles is then presented in Section V. Major conclusions are summarized in Section VI.

II. Formulation and Numerical Scheme

As mentioned in the introduction, we rely on a quasi-1-D, advection-diffusion-reaction design model. The formulation reflects the idealized situation of a dilute solution evolving in a uniform, electrokinetically driven plug flow, and thus inherently ignores dispersive effects that may arise due to unwanted external pressure differences, spatial variation in wall mobility, or spatial variations in electrical conductivity. We consider the evolution of three chemically interacting species using a first-order, finite-rate, reversible reaction of the form

$$A + B \longleftrightarrow C \tag{1}$$

with a chemical rate term given by

$$R_A = R_B = -R_C = -k_f c_A c_B + k_r c_C \tag{2}$$

where the R denotes the rate of production, k_f and k_r denote the forward and backward rates, respectively. The indexes A and B denote the reactants while C refers to the reaction product.

Under the idealized conditions outlined above, the conservation equations for the three reacting species can be expressed as [23]

$$\frac{\partial c_i}{\partial t} + u_i \frac{\partial c_i}{\partial x} = D_i \frac{\partial^2 c_i}{\partial x^2} + R_i, \quad i = A, B, C \tag{3}$$

where c_i, u_i and D_i denote the molar concentration, electromigration velocity, and mass diffusivity of species i, respectively.

In the computations presented in Section IV, (3) is simulated using a finite difference scheme that is based on a cell-centered discretization of the concentration fields on a fine, uniform mesh of cell size Δx. Spatial derivatives are approximated using a second-order, centered-difference discretization, and the discrete equations are advanced in time using the second-order Adams–Bashforth scheme. Inflow/outflow conditions are used at the left/right domain boundaries.

III. Scale Analysis

While the dimensional form of the governing equations is used in the simulations, a brief scale analysis is conducted in this section in order to characterize the solutions. As mentioned earlier, the present study is motivated by a desire to determine rates of reaction in a dilute solution involving proteins having low molecular diffusion coefficients. Thus, molecular diffusion effects are expected to be small, so that the rates of reaction are dominated by electrokinetic and chemical time scales. (For the presently considered regime, diffusion time scales are smaller than crossing time scales by at least three orders of magnitude.) Below, we provide estimates of these time scales, the ratio of which yields a Damköhler number.

A. Electrophoretic Crossing Time Scale

Let w denote the initial widths of species A and B (see Fig. 1). The relevant time scale for band crossing may be estimated from

$$t_{cr} \equiv \frac{w}{\Delta u_{AB}} \tag{4}$$

where $\Delta u_{AB} = u_A - u_B > 0$. The convention we have adopted is that species A with electromigration velocity u_A, is the faster migrating species, which overtakes species B having electromigration velocity u_B.

B. Chemical Time Scale

In order to derive a suitable chemical time scale, we will assume for the moment that the crossing time is fast and consequently consider that the two bands are brought together instantaneously. Thus, we focus on a quasi-0D problem where the initial mixture relaxes to equilibrium. In this limiting case, the relevant concentrations are the initial peak concentrations c_A^0 and c_B^0.

An exact solution to this pure chemical problem can be derived. Since this solution suggests an interesting diagnostic approach, a few details are provided. We use subscripts {1,2,3} to denote species {A,B,C}. In the absence of transport, the governing equation for concentration reduces to

$$\frac{dc_1}{dt} = -k_f c_1 c_2 + k_r c_3. \tag{5}$$

Let $\delta(t)$ denote the amount of reactants consumed by the reaction over the interval $[0, t]$, and Δ denote the steady-state or equilibrium value of δ; we have

$$c_1(t) = c_1^0 - \delta(t), \quad c_2(t) = c_2^0 - \delta(t), \quad c_3(t) = c_3^0 + \delta(t) \tag{6}$$

Substitution of (6) into (5) yields

$$\frac{d\delta}{dt} = k_f c_1^0 c_2^0 - k_r c_3^0 - \delta\left[k_f\left(c_1^0 + c_2^0\right) + k_r\right] + k_f \delta^2. \tag{7}$$

We will later discuss how (7) may be used to diagnose band-crossing data.

At steady state, we have $d\delta/dt = 0$, which gives

$$a\delta^2 - b\delta + c = 0 \tag{8}$$

where $a \equiv k_f$, $b \equiv k_f(c_1^0 + c_2^0) + k_r$, and $c \equiv k_f c_1^0 c_2^0 - k_r c_3^0$. The solution is given by

$$\Delta = \frac{b - \sqrt{b^2 - 4ac}}{2a}. \tag{9}$$

Letting $q(t) = \Delta - \delta(t)$, we have

$$-\frac{1}{2a\Delta - b}\frac{dq}{q} + \frac{a}{2a\Delta - b}\frac{dq}{aq - (2a\Delta - b)} = -dt \tag{10}$$

with initial condition $q(0) = \Delta$. The exact solution is given by

$$q(t) = \frac{\gamma}{a - \theta\exp(-\gamma t)} \tag{11}$$

where $\gamma \equiv 2a\Delta - b = -\sqrt{b^2 - 4ac}$ and $\theta \equiv (b - a\Delta)/\Delta$. As expected, q vanishes at steady-state since $\gamma < 0$, and this is reflected in (11) above.

This suggests that an appropriate timescale, τ, for the reaction is such that $q(\tau) = \Delta/e$, which gives

$$\tau = -\frac{1}{\gamma}\ln\left[\frac{a\Delta - e\gamma}{\theta\Delta}\right]. \tag{12}$$

Note that τ depends on the initial concentrations c_1^0, c_2^0 and, if initially present, c_3^0.

Also note that the above definition of τ differs from the usual definition of the chemical time scale based on the eigenvalues of J, the Jacobian of the chemical source term. For the present reaction mechanism, we have

$$J \equiv \frac{\partial R_i}{\partial c_j} = \begin{vmatrix} -k_f c_2 & -k_f c_1 & k_r \\ -k_f c_2 & -k_f c_1 & k_r \\ k_f c_2 & k_f c_1 & -k_r \end{vmatrix} \tag{13}$$

J has a single nonvanishing eigenvalue $\lambda = -k_f(c_1 + c_2) - k_r$, giving the following timescale:

$$\tau' = \frac{1}{|\lambda|} = \frac{1}{k_f(c_1 + c_2) + k_r} \tag{14}$$

which, unlike τ, does not depend on the initial concentration of the product, c_3^0. However, one can readily verify that for conditions near equilibrium, τ and τ' coincide; this agreement was in fact behind the selection of the $1/e$ decay rate in Δ. In the analysis below, we will exclusively rely on the chemical time scale definition in (12), as it accounts for the overall nonlinear behavior of the system.

C. Damköhler Number

The estimates above enable us to define a Damköhler number

$$\mathrm{Da} \equiv \frac{t_{\mathrm{cr}}}{\tau} \tag{15}$$

In order to control Da one can either alter the initial concentration levels (i.e., control τ), or change the electromigration velocity (i.e., control t_{cr}). The latter can be achieved either by changing the electric field strength or, to the extent possible, by altering w and/or the mobility of individual species. Note, however, that the possibility of experimentally controlling τ and t_{cr} is subject to constraints that limit the range of electromigration velocities and the range of concentration values. For t_{cr}, the primary restriction comes from a limitation on the electric field, which should not be so high as to cause significant Joule heating. For τ, one needs to ensure that the concentration remains high enough to fall within detection limits, but not so high as to require a highly concentrated initial mixture.

IV. Behavior of Solutions

A detailed parametric study was conducted of the effects of electromigration velocities, rate parameters, and initial reactant concentrations. The effects of electromigration velocity were analyzed by systematically varying u_A. For each value of u_A, a two-parameter family of solutions was considered, by setting $u_B = \alpha u_A$ and $u_C = \beta u_A$. The parameter α was varied independently, and for each α, five values of β were considered: 1) $\beta = 0$, where the electromigration velocity of the product vanishes, 2) $\beta = \alpha/2$, i.e., the electromigration velocity of the product (u_C) is half that of the slower reactant (u_B), 3) $\beta = \alpha$, where $u_C = u_B$, 4) $\beta = (1+\alpha)/2$, where $u_C = (u_A + u_B)/2$, and 5) $\beta = 1$, where $u_C = u_A$. Meanwhile, the initial concentrations of the reactants and the values of the rate constants were also systematically varied. In all cases, the width of the initial reactant bands, w, was held fixed, with concentration profiles described by sixth-order Gaussian profiles of the form

$$c_i^0(\xi) = C_i^0 \exp\left(-\frac{\xi_i^6}{w^6}\right), \quad i = A, B$$

where C^0 is the initial peak concentration and ξ is a shifted spatial variable centered at the peak. The high-order Gaussian was selected because it mimics a top-hat profile with smooth tails, as can be appreciated from the results below. In all cases, $w = 50\ \mu\mathrm{m}$, the diffusivity $D = 3 \times 10^{-10}\ \mathrm{m}^2/\mathrm{s}$, the initial product concentration vanishes identically (i.e., $c_C^0 = 0$), and the computational domain is 3-mm long. A systematic study was also conducted of the effect of the discretization parameters. This study showed that for range of parameters of interest, a fine mesh with $\Delta x = 0.2\ \mu\mathrm{m}$ and a time step $\Delta t = 10\ \mu\mathrm{s}$ were sufficient for accurate predictions. These values are used in the computations presented below.

Selected cases from the detailed parametric study are presented in this section. As summarized in Table I, we focus our attention on six cases. In cases 1–4, the electromigration velocity of the reactants is held fixed, while that of the products is varied. Thus, as shown in the table, the Damköhler number and α are held fixed, respectively $\mathrm{Da} = 33$ and $\alpha = 0.25$, while β is varied. In case 5, α is increased to 0.5, resulting in a higher Damköhler number $\mathrm{Da} = 49$. In case 6, the initial peak concentration of the reactants is reduced, leading to a lower Damköhler number $\mathrm{Da} = 2$.

Fig. 2 depicts the evolution of the reactants' concentration profiles for case 1 (see Table I). The results illustrate how the two bands approach each other in the early stage of the computation. Due to weak molecular diffusion effects, before the two bands overlap, there is little change in the peak concentration of

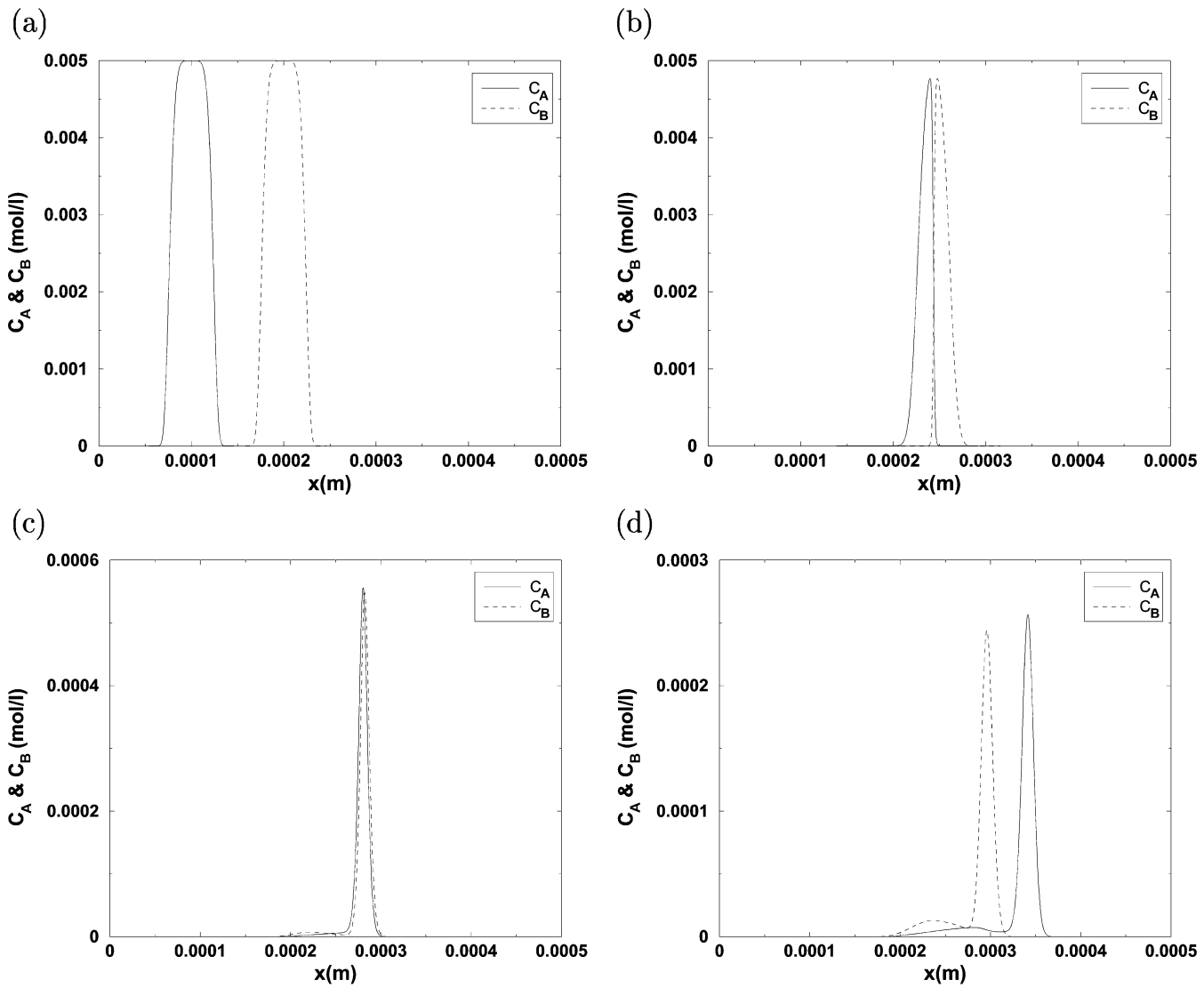

Fig. 2. Instantaneous profiles of C_A and C_B for case 1. Plots are generated at times (a) $t = 0$, (b) $t = 50\,\mathrm{ms}$, (c) $t = 70\,\mathrm{ms}$, and (d) $t = 90\,\mathrm{ms}$.

TABLE I
SELECTED INPUT CASES. SHOWN ARE VALUES OF THE ELECTROMIGRATION VELOCITIES (mm/s), INITIAL REACTANT CONCENTRATIONS (mM), FORWARD REACTION RATE ($\mathrm{M^{-1}s^{-1}}$), AND BACKWARD REACTION RATE ($\mathrm{s^{-1}}$). ALSO SHOWN ARE THE DIMENSIONLESS PARAMETERS α AND β AS WELL AS THE DAMKÖHLER NUMBER, Da

Case	u_A	u_B	u_C	C_A^0	C_B^0	k_f	k_r	α	β	Da
1	3	0.75	0	5.	5.	4×10^5	0.1	0.25	0	33
2	3	0.75	0.375	5.	5.	4×10^5	0.1	0.25	0.125	33
3	3	0.75	0.75	5.	5.	4×10^5	0.1	0.25	0.25	33
4	3	0.75	1.875	5.	5.	4×10^5	0.1	0.25	0.625	33
5	3	1.5	1.5	5.	5.	4×10^5	0.1	0.5	0.5	49
6	3	0.75	0.75	0.25	0.25	4×10^5	0.1	0.25	0.25	2

A and B. For these conditions, the peak concentrations of A and B decrease rapidly when the two bands overlap, and by the time the bands separate, the peak concentrations drop by approximately a factor of 20. As shown in Fig. 2(d), after separation the reactant profiles are no longer symmetric and slight differences in the peak concentrations of A and B can be observed. The profiles exhibit a double hump structure with a strong primary peak that leads a weak local maximum. The behavior of the reactants concentration profiles for cases 2–4 was found to be qualitatively similar to that of Case 1; the corresponding plots are consequently omitted.

Fig. 3 shows instantaneous profiles of C_A and C_B for case 5. As shown in Table I, for this case, β has been increased to 0.5, which results in an increased crossing time scale and, consequently, a larger Damköhler number. The results indicate the profiles of C_A and C_B behave in a qualitatively similar fashion as in case 1 (Fig. 2). However, for case 5, there is an even more substantial reduction in the peak values of C_A and C_B, which drop by approximately a factor of 30 during the crossing. As further discussed below, this suggests that the overall rate of progress of the reaction is larger as Da increases.

As shown in Table I, the electromigration velocities for case 6 are the same as in case 3, but the initial concentrations of A and B have been reduced by a factor of 20. This results in a significant drop in the Damköhler number, from $\mathrm{Da} = 33$ in case 3 to $\mathrm{Da} = 2$ in case 6. Instantaneous profiles of C_A and C_B for case 6 are plotted in Fig. 4, using the same time intervals as in Fig. 2. The plots show that for case 6, the behavior of the reactants' profiles differs significantly from that of the

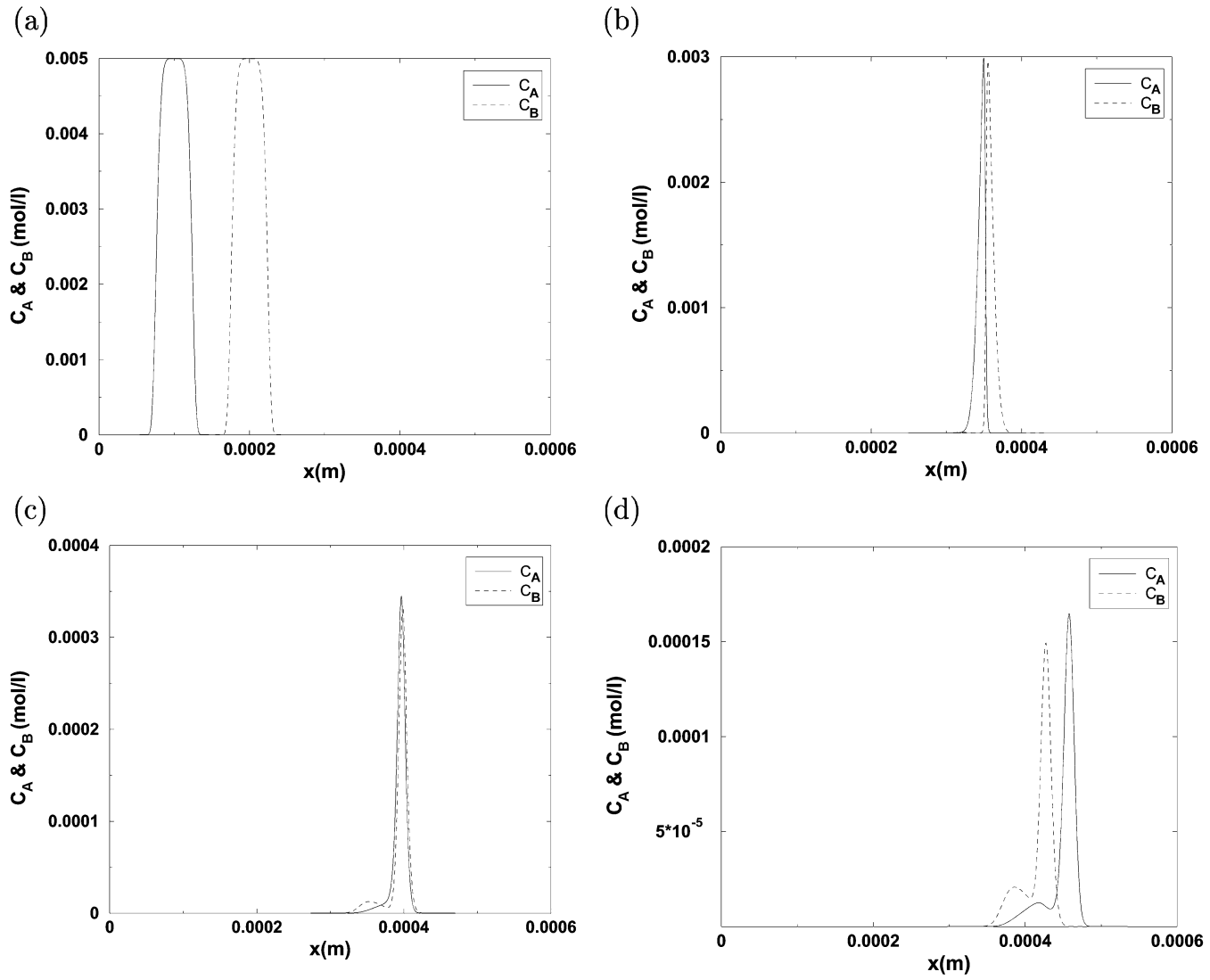

Fig. 3. Instantaneous profiles of C_A and C_B for case 5. Plots are generated at times (a) $t = 0$, (b) $t = 90\,\mathrm{ms}$, (c) $t = 110\,\mathrm{ms}$, and (d) $t = 130\,\mathrm{ms}$.

previous cases. Specifically, the concentration profiles develop a weak asymmetry and, unlike the profiles in Figs. 2 and 3, do not exhibit a secondary trailing peak. An additional distinctive feature is the prolonged coexistence of C_A and C_B during the crossing [see Fig. 4(b)]. As expected, for this reduced value of Da, the drop in the peak concentrations of A and B is rather weak, approximately a factor of 3.

The effects of electromigration velocities and Damköhler number can also be observed in Fig. 5(a)–(f), which depicts the evolution of product concentration profiles for cases 1–6, respectively. As shown in Table I, for cases 1–4, Da and the electromigration velocities of the reactants are held fixed, while u_C is systematically varied by increasing α. For $\alpha = 0$, u_C vanishes so that the product concentration profiles does not propagate. As shown in Fig. 5(a), at the beginning of band crossing $(t = 50\,\mathrm{ms})$ the product concentration profile exhibits a sharp leading front, followed by a smoothly decaying tail. As the reaction proceeds, the leading front becomes smoother, eventually giving the profile a nearly symmetric shape. For the present case $(u_C = 0)$, the product concentration profile has an appreciably smaller peak and larger width than the initial reactants' profile.

A similar behavior is observed in Fig. 5(b), which depicts the evolution of c_C for case 2, where $u_C = u_B/2$. However, one can observe that for this case the final profile has smaller width and higher peak than in case 1. Furthermore, unlike case 1, the C_C profile is no longer stationary, but translates to the right with the product electromigration velocity u_C.

The trends noted above can also be observed for case 3, where $u_C = u_B$. In particular, as shown in Fig. 5(c), the product concentration profile for case 3 has slightly larger peak and is slightly thinner than in the previous cases. In particular, for case 3 the peak product concentration following the band crossing is close to that of the initial reactants profiles.

When u_C is equal to the average of u_A and u_B (case 4), a peculiar behavior is observed. As shown in Fig. 5(d), a very narrow profile with a pronounced peak is observed. Note that the peak concentration is more than 4 times higher than initial peak of the reactants profiles. Thus, in the present situation the product tends to accumulate at a single spatial position that moves with the average velocity of the reactants. We finally note that, if u_C is increased further then the presently observed "focusing" effect is greatly diminished. In these cases, i.e. $u_C > (u_A + u_B)/2$, the product concentration resembles

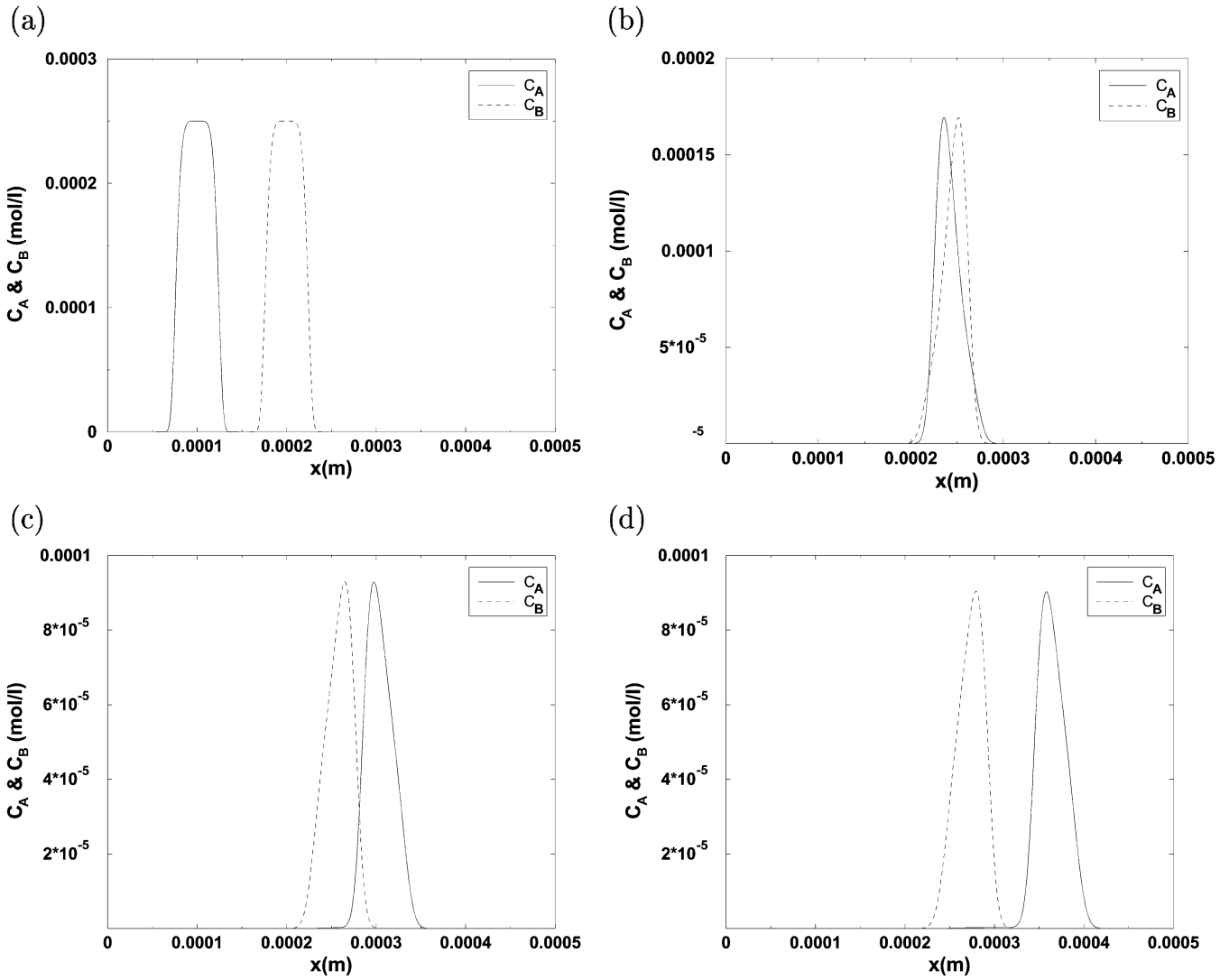

Fig. 4. Instantaneous profiles of C_A and C_B for case 6. Plots are generated at times (a) $t = 0$, (b) $t = 50$ ms, (c) $t = 70$ ms, and (d) $t = 90$ ms.

those in Fig. (5a)–(c); the corresponding results are therefore omitted.

Fig. 5(e) shows instantaneous product concentration profiles for case 5. Compared with case 3, in case 5 the velocities u_B and u_C have been doubled. This results in a longer crossing time scale and consequently a larger Damköhler number. As can be seen in Fig. 5(c) and (e), however, these changes appear to have little impact on the shape of the product concentration profiles. While interaction times evidently differ, in both cases the profiles develop similar widths and peak values.

Finally, concentration profiles for case 6 are shown in Fig. 5(f). As shown in Table I, the electromigration velocities are identical in cases 3 and 6, but the initial reactants concentrations are substantially lower in case 6. As a result, in the latter case the Damköhler number is significantly lower. The reduction in Damköhler number appears to have little impact on the shape of the profiles, but does have a noticeable effect on the rate of progress of the reaction. Specifically, in case 3 the peak product concentration is nearly equal to the initial reactants' peak, while the peak product concentration in case 6 is noticeably lower.

The above results indicate that the behavior of the concentration profiles can be essentially characterized by the Damköhler number, and by the ratio of the electromigration velocity of the product with respect to the mean of the reactants electromigration velocities. The trends with these two parameters, briefly illustrated above for selected cases, were in fact observed for a wide range of electromigration velocities, rate constants, and initial concentrations.

In order to briefly illustrate the above claims, we compute two measures that characterize the progress of the reaction: a global measure $\mathcal{G}$ defined by

$$\mathcal{G} \equiv \max_t \frac{\int c_C \mathrm{d}x}{\int c_A^0 \mathrm{d}x} \tag{16}$$

and a local measure $\mathcal{P}$ given by

$$\mathcal{P} \equiv \max_t \frac{c_C^{\max}(t)}{c_A^{\max}(t=0)}. \tag{17}$$

Here, $c_A^{\max}$ and $c_C^{\max}$ denote the peak instantaneous values of the concentrations of A and C, respectively. Note that $\mathcal{G}$

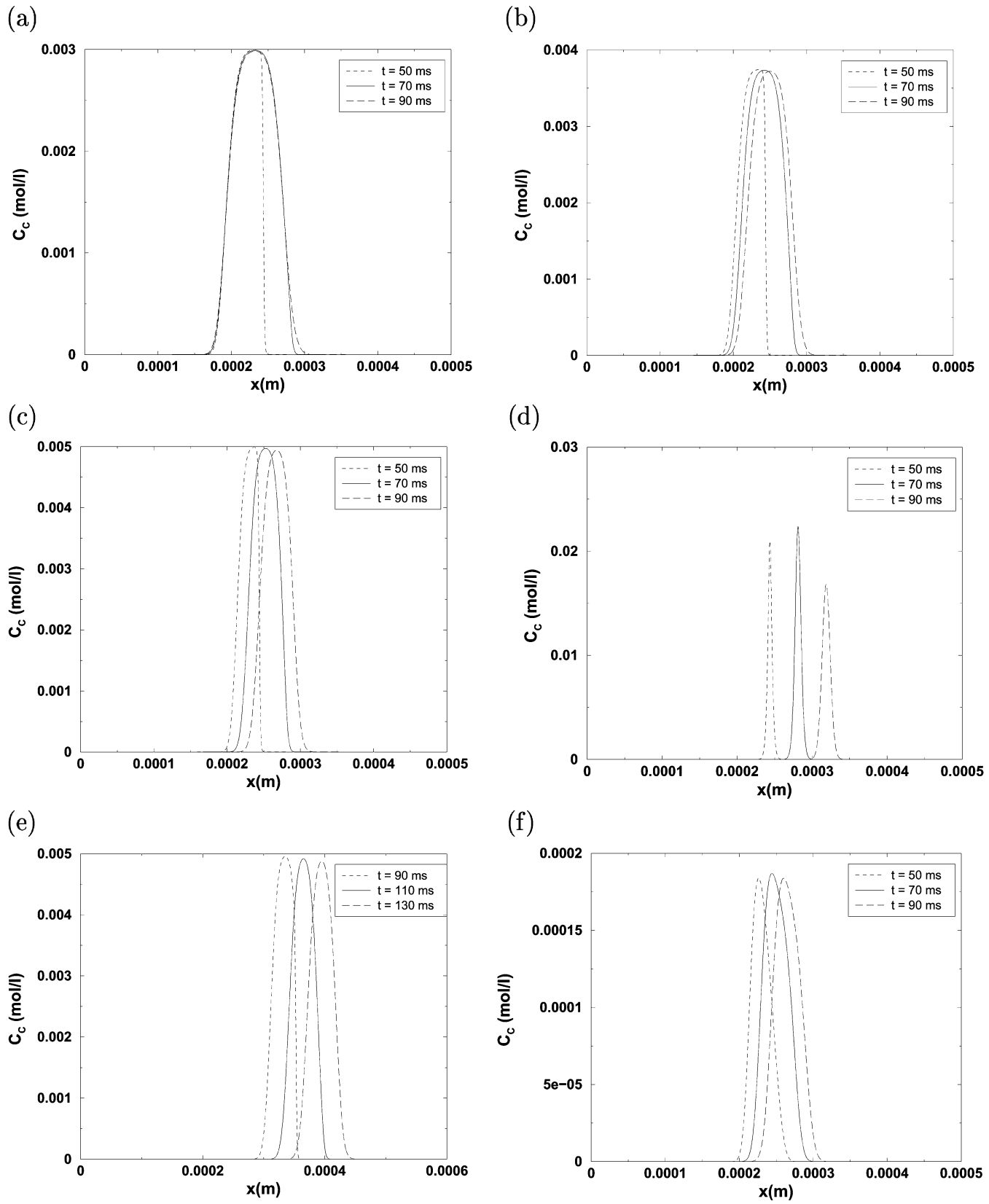

Fig. 5. Instantaneous profiles of C_C for cases (a) 1, (b) 2, (c) 3, (d) 4, (e) 5, and (f) 6.

can be interpreted as "chemical conversion efficiency" since it corresponds to the peak fraction of moles of A that are converted into moles of C by the chemical reaction. On the other hand, $\mathcal{P}$ corresponds to the peak spatial product concentration normalized by the initial peak of the concentration profile of A. Thus, it reflects the tendency of the peak product concentration to be larger or smaller than the initial peak of the reactants.

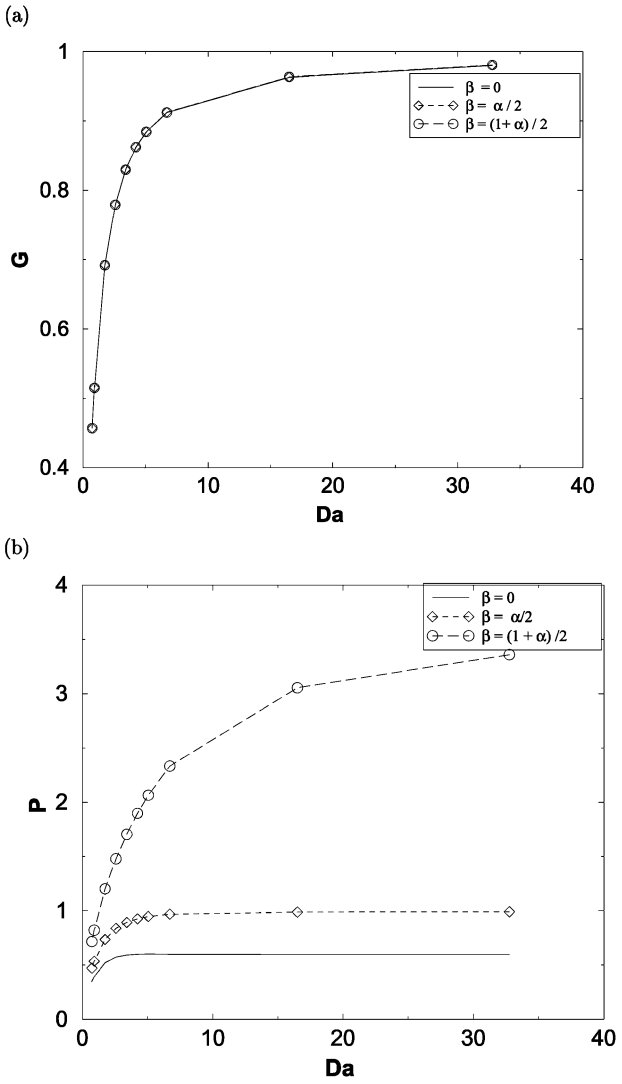

Fig. 6. Dependence of $\mathcal{G}$ (top) and $\mathcal{P}$ (bottom) on Da. Different curves are generated for cases with $\beta = 0$, $\alpha/2$, and $(1+\alpha)/2$.

Fig. 6(a) shows the dependence of $\mathcal{G}$ on the Damköhler number. Plotted are curves generated for $\beta = 0$, $\alpha/2$ and $(1+\alpha)/2$, and for Damköhler numbers in the range $1 \leq \mathrm{Da} \leq 33$. The figure shows that the three $\mathcal{G}$ versus Da curves collapse onto each other, supporting the earlier claim that the overall conversion of reactants into products is governed by the Damköhler number, and is essentially independent of the ratios of electromigration velocities. Note that the curves for $\mathcal{G}$ are monotonically increasing, from about 45% at low Da to about 98% at higher Da. Thus, as observed earlier, consumption of the reactants increases with increasing Damköhler numbers.

Meanwhile, as shown in Fig. 6(b), distinct $\mathcal{P}$ versus Da curves are obtained for each value of β. For all three values of β, the curves increase monotonically with Da. For $\beta = 0$ and $\alpha/2$, the curves saturate for $\mathrm{Da} > 10$, while for $\beta = (1+\alpha)/2$ substantial variation is observed throughout the range considered. The largest values of $\mathcal{P}$ are achieved when $\beta = (1+\alpha)/2$, i.e. when the product electromigration velocity is equal to the average of the electromigration velocities of the reactants. In particular, for this value of β, $\mathcal{P}$ is substantially larger than unity at high Da; this indicates that in this regime the peak product concentration is several times larger than the peak reactant concentration.

We finally note that the results in Fig. 6 are consistent with earlier observations of the behavior of the concentration profiles, and their dependence on relevant parameters. In addition, the results enable us to generalize previously observed trends to a wider range of operating conditions.

V. Estimation of Rate Constants

We now explore the possibility of extracting reaction rates from the evolution of concentration profiles. This exercise is motivated by optical measurements of species concentrations, which give spatial profiles at selected time intervals [24]. In many cases, the impact of experimental noise may be reduced by analyzing moments of the profile instead of local values. In this section, we examine two different means for exploiting such integral measures. In the first approach (see Section V-A), concentration profiles of both reactants and of the product are assumed available. A different scenario is considered in Section V-B, which involves interrupting the electric field once the bands overlap. For this scenario, an alternative means of estimating chemical rate constants is considered which only assumes that the reactants' concentration profiles are measured.

A. Multiple Measurements

When the concentrations of both reactants and of the product are simultaneously measured, a simple approach can be implemented to deduce the reaction rates. Specifically, by integrating (3) over the domain or, in the case of experimental measurements, over a sufficiently wide window, the transport (convection, electromigration and diffusion) terms drop out, and one obtains

$$I_1(t) \equiv \frac{d}{dt}\int c_1 = -k_f \int c_1 c_2 + k_r \int c_3. \qquad (18)$$

If the signals for $I_1(t)$, $\int c_1 c_2$ and $\int c_3$ are available, then one can perform a straightforward least-squares regression of the form

$$I = -A\int c_1 c_2 + B\int c_3 \qquad (19)$$

to determine unknown coefficients A and B. These can be immediately identified with k_f and k_r. In particular, based on the computed results for case 3 we obtain $A = 3.99 \times 10^5$ and $B = 0.088$. These values are in very good agreement with the rate parameters used as input. Similar experience was observed for other cases considered; the corresponding results are therefore omitted.

B. Interrupted Flow Experiment

In many situations, simultaneous measurement of all three species concentrations is either not possible or excessively difficult. In this section, we explore the possibility of deducing reaction rates with fewer experimental signals. Specifically, we consider what we call an "interrupted flow" experiment, which consists of first driving the reactants so that they overlap and then suddenly switching off the electrokinetic pumping (see also

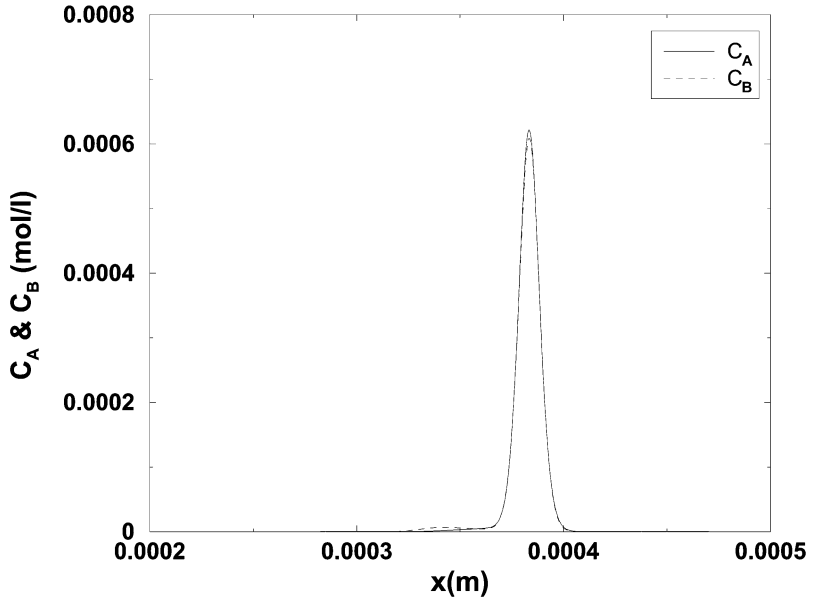

Fig. 7. Profiles of reactants concentration at the time the flow is interrupted.

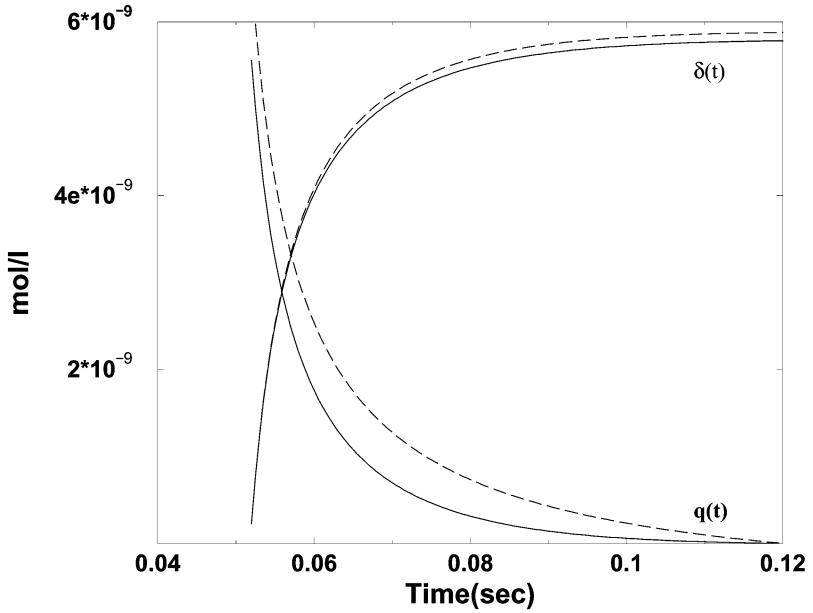

Fig. 8. Comparison of analytical (dashed) and numerical (solid) results for $\delta(t)$ and $q(t)$.

[16], [17]). The advantage of this approach is that, in the parameter regime of interest, once the flow is interrupted, the evolution of the concentration fields is primarily dominated by the reaction and only weakly affected by diffusion. The assumptions will be verified based on simulation results below.

The simulation conditions are the same as those in the previous section. However, once the reactants overlap, all velocities are suddenly switched to zero. The reactant concentration profiles at the time the flow is interrupted are shown in Fig. 7. This mimics the sudden interruption of the electric field since, due to the very low Reynolds number and the absence of a driving pressure gradient, the bulk velocity decays rapidly to zero.

We start by examining the effects of diffusion on the evolution of the concentration field. In Fig. 8, we contrast the computed values of $\delta(t)$ and $q(t)$ at the location of the peak reactant concentration (see Fig. 7) to the analytical solution for a purely reactive system [see (11)]. The results show that the two predictions are in reasonably close agreement, indicating that for the present set of conditions diffusion has a small effect on the evolution of $\bar{q}$ and $\bar{\delta}$ throughout the decay period.

Combined with the weak effect of diffusion, the absence of advective or electromigration effects then offers the following possibility of extracting the reaction rates. From (7) we have

$$\frac{d\delta}{dt} = k_f c_1^0 c_2^0 - k_r c_3^0 - \delta\left[k_f\left(c_1^0 + c_2^0\right) + k_r\right] + k_f\delta^2. \quad (20)$$

Integrating over a fixed, sufficiently large window, we have:

$$\int \frac{d\delta}{dt}\mathrm{d}x = -k_r \int \delta \mathrm{d}x + k_f \int \left[\delta^2 - \left(c_1^0 + c_2^0\right)\delta\right]\mathrm{d}x + \int \left[k_f c_1^0 c_2^0 - k_r c_3^0\right]\mathrm{d}x \quad (21)$$

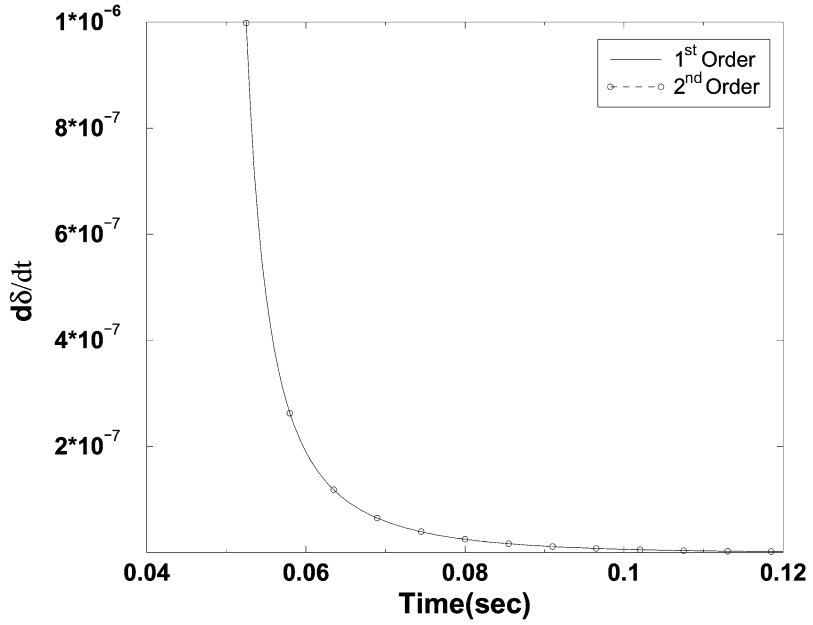

Fig. 9. Evolution of $(d\bar{\delta}/dt)$ using first and second-order approximations. The time step used in the finite difference formulae corresponds to that of the simulations, i.e., $\Delta t = 10^{-5}$ s.

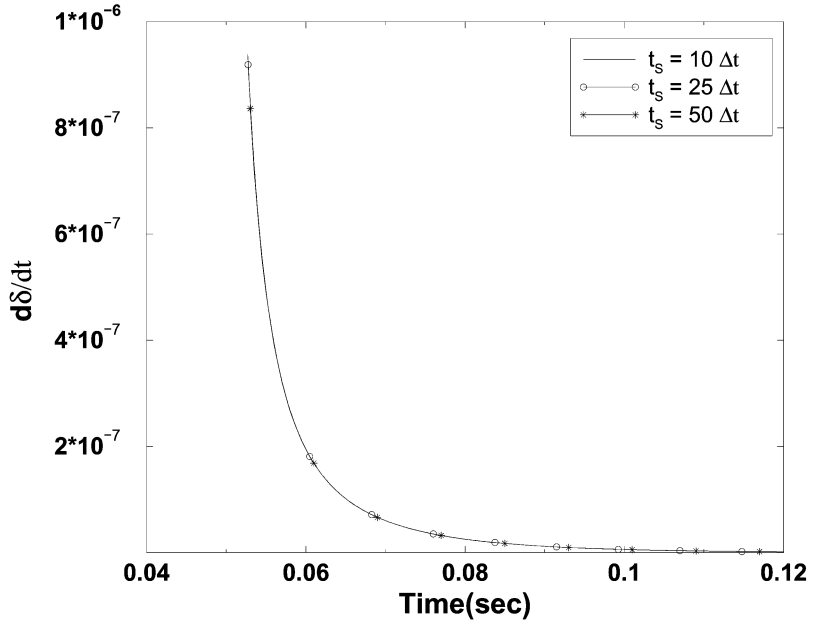

Fig. 10. Evolution of $(d\delta/dt)$ using a second-order approximation. The time step used in the finite difference formula corresponds to the length of the sampling interval, t_s. We use $t_s = 10\Delta t, 25\Delta t$ and $50\Delta t$.

which can be rewritten as

$$\frac{d\bar{\delta}}{dt} = -A\bar{\delta} + B\int \left[\delta^2 - \left(c_1^0 + c_2^0\right)\delta\right] \mathrm{d}x + C \qquad (22)$$

where $\bar{\delta} \equiv \int \delta \mathrm{d}x$. Thus, if time resolved measurements evolution of one reactant concentration are performed, and the "initial" concentration of the other reactant is also measured, one can determine the coefficients A, B, and C by linear regression (least-squares) from the data. Comparing (21) and (22), one can immediately identify the coefficients A and B with the backward rate and forward rate, respectively.

TABLE II
LEAST-SQUARES INTERPOLATION RESULTS USING THE ANALYTICAL SOLTUTION FOR A PURELY REACTIVE SYSTEM

Coefficients	$t_s = 50\Delta t$	$t_s = 25\Delta t$
A	0.1002	0.1000
B	4.0000×10^{5}	4.0000×10^{5}
C	4.3363×10^{-6}	4.3363×10^{-6}

Note, however, that unlike the approach of the previous section, the present approach is only approximate, and its success hinges on situations where Da is not so large that the reactants are consumed very quickly (see Fig. 6), before one can inter-

TABLE III
LEAST-SQUARES INTERPOLATION RESULTS FOR DIFFERENT SAMPLING TIMES t_s USING THE COMPUTED SOLUTIONS. SHOWN ARE RESULTS OBTAINED WHEN MOLECULAR DIFFUSION ACCOUNTED FOR ($D \neq 0$) AND WHEN IT IS IGNORED ($D = 0$). IN THE PRESENT CASE, ESTIMATES OF $d\bar{\delta}/dt$ ARE OBTAINED FROM A CENTERED DIFFERENCE APPROXIMATION USING THE COMPUTATIONAL TIME STEP Δt

Coefficients	$D = 0$			$D \neq 0$		
	$t_s = 50\Delta t$	$t_s = 25\Delta t$	$t_s = 10\Delta t$	$t_s = 50\Delta t$	$t_s = 25\Delta t$	$t_s = 10\Delta t$
A	0.1012	0.1011	0.1023	0.275	0.2712	0.2676
B	4.0000×10^{5}	4.0000×10^{5}	3.9999×10^{5}	3.9963×10^{5}	3.9964×10^{5}	3.9965×10^{5}
C	1.2970×10^{-6}	1.2970×10^{-6}	1.2970×10^{-6}	1.2969×10^{-6}	1.2969×10^{-6}	1.2969×10^{-6}

TABLE IV
LEAST-SQUARES INTERPOLATION RESULTS FOR DIFFERENT SAMPLING TIMES t_s USING THE COMPUTED SOLUTIONS. SHOWN ARE RESULTS OBTAINED WHEN MOLECULAR DIFFUSION ACCOUNTED FOR ($D \neq 0$) AND WHEN IT IS IGNORED ($D = 0$). IN THE PRESENT CASE, ESTIMATES OF $d\bar{\delta}/dt$ ARE OBTAINED FROM A CENTERED DIFFERENCE APPROXIMATION USING THE SAMPLING TIME t_s

Coefficients	$D = 0$			$D \neq 0$		
	$t_s = 50\Delta t$	$t_s = 25\Delta t$	$t_s = 10\Delta t$	$t_s = 50\Delta t$	$t_s = 25\Delta t$	$t_s = 10\Delta t$
A	3.7046	1.0067	0.2532	3.9915	1.2094	0.4247
B	3.8619×10^{5}	3.9661×10^{5}	3.9944×10^{5}	3.8537×10^{5}	3.9613×10^{5}	3.9908×10^{5}
C	1.2732×10^{-6}	1.2913×10^{-6}	1.2961×10^{-6}	1.2719×10^{-6}	1.2909×10^{-6}	1.2960×10^{-6}

rupt the flow. Also, note that if pointwise, time-resolved measurements are sufficiently accurate, the regression analysis can be performed on (20) directly. In this case pointwise measurement of only a single reactant concentration is needed, with the coefficient of δ^2 providing k_f. This latter possibility, however, is not explored in the present study.

The evolution of $d\bar{\delta}/dt$ is shown in Figs. 9 and 10. In Fig. 9, we rely on first- and second-order formulas for evaluating the derivative, and in both cases the time step corresponds to that used in the computations. In Fig. 10, we rely only on a second-order approximation, with a sampling time step t_s that is significantly larger than that used in the computations. This mimics actual experiments, where sampling at very high frequencies may neither be possible nor desirable. As shown in the figures, in all cases $d\bar{\delta}/dt$ is well approximated.

The least-squares procedure is tested using the analytical solution for a purely reactive system at different sampling time intervals. As shown in Table II the interpolated coefficients match the actual input parameters $k_f = 4 \times 10^5$ and $k_r = 0.1$. Note, however, that at the larger sampling interval very small errors appear in the estimate of k_r, even though the exact solution is used as input to the regression. These weak errors reflect the amplification of round-off errors due to the stiffness of the linear equation system. As further discussed below, the impact of this stiffness is substantially more pronounced when numerical results are used, especially when molecular diffusion effects are accounted for.

We now apply the regression analysis directly to the output of the computations. The analysis is conducted in two versions. In the first version, we simply switch off the electric field, as outlined above. In the second, both diffusion and electromigration are interrupted. Comparison of the two sets of results thus enables us to directly assess the role of diffusion on the extrapolated rates.

As shown in (22), the present analysis requires estimates of $d\bar{\delta}/dt$. In the results below, these estimates are obtained using a second-order centered-difference formula. In the results shown in Table III, this approximation is performed within the simulations, using the computational time step $\Delta t = 10\ \mu$s. The sampling time, t_s, denotes the time interval between neighboring points in the least-squares procedure. Thus, in Table III, the derivative $d\bar{\delta}/dt$ is estimated using a finer time step than the sampling time t_s. In Table IV, this exercise is repeated with $d\bar{\delta}/dt$ estimated from the sampled data, i.e., using a time step equal to the sampling time t_s. This latter case mimics more closely the experimental analysis, as data between neighboring points is not available.

Examination of the results in Tables III and IV indicates that:

1) There is better agreement between the estimated and input/known values ($k_f = 4 \times 10^5$, $k_r = 0.1$) of the reaction rates for the case where the derivative $d\bar{\delta}/dt$ is estimated based on the computational time step. Thus, for fixed t_s, the agreement between the estimated and input values deteriorates when the derivative is estimated on a wider time interval.
2) Kinetic rate estimates obtained with molecular diffusion ignored are in better agreement with the input values than estimates obtained in the diffusive cases. This indicates that even though diffusion may have weak a effect on the absolute values of concentration, it still has a substantial effect on the least-squares predictions, especially at large sampling intervals.
3) The extrapolated backward rate is highly sensitive to the presence of diffusion and to the sampling interval t_s. Except for small t_s and negligible diffusion, the interrupted flow approach proposed here does not seem to be a practical method of estimating the backward rate, k_r. The high-sensitivity of the estimated values of k_r can be traced to the stiffness of the equation system, which leads to an ill-conditioned matrix.
4) In contrast, the extrapolated values of k_f are much more robust, and provide reasonable estimates of the forward rate. In particular, for all cases analyzed, the estimated value of k_r differs by less than 4% from the input value.

VI. Conclusion

A numerical study of band-crossing reactions was conducted using a quasi-1-D computational model. The model accounts for the evolution of species concentrations due to bulk advection, electromigration, diffusion and chemical reaction. The latter is described using a single step, reversible mechanism involving two reactants and one product. Attention is focused on a fast reaction between initially unmixed bands.

A parametric study of the behavior of the species profiles during the crossing was performed. Simulation results were interpreted in terms of the Damköhler number and of the ratios of the electromigration velocities of the reactant and product. As expected, the results indicate that the overall consumption of the reactants increases as the Damköhler number increases. The results also indicate that the structure of the concentration profile is strongly dependent on the differences of electromigration velocities. In particular, when the product electromigration velocity is equal to the average of the reactants electromigration velocities, the product concentration exhibits a thin profile with peak values significantly higher than the initial reactants' concentrations. This stacking effect may provide a useful means of sample preconcentration based on reaction rates and mobilities, and for enhancing the sensitivity of a variety of on-chip assays. For higher or lower velocity, the product concentration profiles are spatially wider and exhibit significantly lower peak values.

The simulations were then used to explore the possibility of extracting forward and backward rates based on time resolved observation of integral moments of species concentrations. When signals of all three species are observed, a robust extraction procedure can be implemented, which results in excellent estimates of the forward and reverse rates. The simulations are also used to investigate interrupted flow experiments where only the reactants' concentrations are measured. In these situations, an approximate analysis can be applied to extract reaction rate parameters. Results indicate that in the case of fast forward reaction this approach yields robust estimates of the forward rate constant, but that the reverse rate parameter is not accurately predicted.

References

[1] L. Bousse, C. Cohen, T. Nikiforov, A. Chow, A. R. Kopf-Sill, R. Dubrow, and J. W. Parce, "Electrokinetically controlled microfluidic analysis systems," *Annu. Rev. Biophys. Biomol. Struct.*, vol. 29, pp. 155–181, 2000.

[2] P. Yager, Basic Microfluidic Concepts, 2001.

[3] A. E. Kamholz, B. H. Weigl, B. A. Finlayson, and P. Yager, "Quantitative analysis of molecular interaction in a microfluidic channel: the t-tensor," *Anal. Chem.*, vol. 71, pp. 5340–5347, 1999.

[4] A. G. Hadd, D. E. Raymond, J. W. Halliwell, S. C. Jacobson, and J. M. Ramsey, "Microchip device for performing enzyme assays," *Anal. Chem.*, vol. 69, pp. 3407–3412, 1997.

[5] A. G. Hadd, S. C. Jacobson, and J. M. Ramsey, "Microfluidic assays aof acetylcholnesterase inhibitors," *Anal. Chem.*, vol. 71, pp. 5206–5212, 1999.

[6] P. Galambos, PhD thesis, Department of Mechanical Engineering, University of Washington, Seattle, WA, 1998.

[7] N. Chiem and D. J. Harrison, "Microchip-based capillary electrophoresis for immunoassays: analysis of monoclonal antibodies and theophylline," *Anal. Chem.*, vol. 69, pp. 373–378, 1997.

[8] ——, "Microchip systems for immunoassay: an integrated immunoreactor with electrophoretic separation for serum theophylline determination," *Clin. Chem.*, vol. 44, pp. 591–598, 1998.

[9] B. K. Lance, D. Schmalzing, A. T. Todd, and M. Fuchs, "Microchip electrophoretic immunoassay for serum cortisol," *Anal. Chem.*, vol. 68, pp. 18–22, 1996.

[10] G. B. Lee, S. H. Chen, G. R. Huang, W. C. Sung, and Y. H. Lin, "Microfabricated plastic chips by hot embossing methods and their applications for dna separations and detection," *Sens. Actuators, Chem. B*, vol. 75, pp. 142–148, 2001.

[11] I. K. Glaskow *et al.*, "Handling individual mammalian embryos using microfluidics," *IEEE Trans. Biomed. Eng.*, vol. 48, pp. 570–578, 2001.

[12] J. Kameoka, H. G. Craighead, H. W. Zhang, and J. A. Helion, "A polymeric microfluidic chip for ce/ms determination of small molecules," *Anal. Chem.*, vol. 73, pp. 1935–1941, 2001.

[13] T. J. Johnson, D. Ross, and L. E. Locascio, "Rapid microfluidic mixing," *Anal. Chem.*, vol. 74, pp. 45–51, 2002.

[14] B. He, B. J. Burke, X. Zhang, R. Zhang, and F. E. Regnier, "A picoliter-volume mixer for microfluidic analysis systems," *Anal. Chem.*, vol. 73, pp. 1942–1947, 2001.

[15] M. H. Oddy, J. G. Santiago, and J. C. Mikkelsen, "Electrokinetic instability micromixing," *Anal. Chem.*, vol. 73, pp. 5822–5832, 2001.

[16] J.Jianmin Bao and F. E.Fred E. Regnier, "Ultramicro enzyme assays in a capillary electrophoretic system," *J. Chromatogr.*, vol. 608, pp. 217–224, 1992.

[17] B. J.Bryan J. Harmon, D. H.Dale H. Patterson, and F. E.Fred E. Regnier, "Mathematical treatment of electrophoretically mediated microanalysis," *Anal. Chem.*, vol. 65, pp. 2655–2662, 1993.

[18] C. H. Chen, J. C. Mikkelsen, and J. G. Santiago, "Electrophoretic band crossing for measurements of biomolecular binding kinetics," presented at the 2000 International Forum on Biochip Technologies, Beijing, China.

[19] J. B. Knight, A. Vishwanath, J. P. Brody, and R. H. Austin, "Hydrodynamic focusing on a silicon chip: mixing nanoliters in microseconds," *Phys. Rev. Let.*, vol. 80, pp. 3863–3866, 1998.

[20] B. J. Harmon, I. Leesong, and F. E. Regnier, "Selectivity in electrophoretically mediated microanalysis by control of product detection time," *Anal. Chem.*, vol. 66, pp. 3797–3805, 1994.

[21] ——, "Moving boundary electrophoretically mediated microanalysis," *J. Chromatogr. A*, vol. 726, pp. 193–204, 1996.

[22] D. H.Dale H. Patterson, B. J.Bryan J. Harmon, and F. E.Fred E. Regnier, "Dynamic modeling of electrophoretically mediated microanalysis," *J. Chromatogr. A*, vol. 732, pp. 119–132, 1996.

[23] V. P. Andreev and N. S. Pliss, "Computer simulation of electroinjection analysis and electrophoretically mediated microanalysis commensurable concentrations of sample and reagent," *J. Chromatogr. A*, vol. 845, pp. 227–236, 1999.

[24] S. Devasenathipathy and J. G. Santiago, "Electrokinetic flow diagnostics," in *Micro- and Nano-Scale Diagnostic Techniques*. New York: Springer, 2002.

Alain Matta received the B.E. degree in civil engineering from the Lebanese American University, Lebanon, in 2000 and the M.S. degree in civil engineering from the Johns Hopkins University (JHU), Baltimore, MD, in 2003. He is currently working toward the Ph.D. degree in the Department of Civil Engineering at JHU.

His research focuses on stochastic modeling of microfluidic systems.

Omar M. Knio received the Ph.D. degree in mechanical engineering from the Massachusetts Institute of Technology (MIT), Cambridge, in 1990.

He is Professor of Mechanical Engineering at the Johns Hopkins University (JHU), Baltimore, MD. He held a Postdoctoral Associate position at MIT, before joining the Mechanical Engineering Faculty at JHU in 1991. His research interests include computational fluid mechanics, oceanic and atmospheric flows, turbulent flow, physical acoustics, chemically reacting flow, energetic materials, microfluidic devices, dynamical systems, as well as asymptotic and stochastic techniques.

Roger G. Ghanem received both the Master's and Ph.D. degrees from Rice University, Houston, TX.

He is Professor of Civil Engineering at the Johns Hopkins University (JHU), Baltimore, MD, where he specializes in the area of computational stochastic mechanics on which has authored numerous publications.

Chuan-Hua Chen received the B.S. degree in mechanics from Beijing University, China, and the M.S. degree in mechanical engineering from Stanford University, Stanford, CA. He is currently working toward the Ph.D. degree and is a Research Assistant at the Stanford Microfluidics Laboratory, where his research involves electrokinetic microsystems. He has published on electroosmotic micropumps, bioreaction kinetics, and electrokinetic flow instabilities.

Juan G. Santiago received the Ph.D. degree in mechanical engineering from the University of Illinois at Urbana-Champaign (UIUC).

He was a Senior Member of the Technical Staff at the Aerospace Corporation from 1995 to 1997, where his work included the development of flow diagnostics for micronozzles. He was then a Research Scientist at UIUC's Beckman Institute from 1997 to 1998, where he studied the performance of scaled down bioanalytical microfluidic systems. Since 1998, he has been an Assistant Professor of Mechanical Engineering at Stanford University, Stanford, CA, where he specializes in microscale fluid mechanics, microscale optical flow diagnostics, and microfluidic system design. His research includes the investigation of transport phenomena and optimization of systems involving microscale fluid pumping, electrophoretic injections and separations, sample concentration methods, and rapid micromixing processes. The applications of this research include microfabricated bioanalytical systems for drug discovery and bioweapon detection. He is the Director of the Stanford Microfluidics Laboratory.

Bert Debusschere received the M.S. and Ph.D. degrees in mechanical engineering from the University of Wisconsin—Madison in 1995 and 2001, respectively, and the B.S. degree in mechanical engineering from the Katholieke Universiteit Leuven, Belgium, in 1994.

He is a Research Associate at Sandia National Laboratories, Livermore, CA. His research interests include simulation of turbulent scalar transport, microfluidic flow phenomena, and stochastic uncertainty quantification.

Habib N. Najm received the M.S. and Ph.D. degrees in mechanical engineering from the Massachusetts Institute of Technology (MIT), Cambridge, in 1986 and 1989, respectively, and the B.E. degree in mechanical engineering from the American University of Beirut in 1983.

He is a Principal Member of the Technical Staff at Sandia National Laboratories in Livermore, CA. Before joining Sandia in 1993, he worked with the Semiconductor Process Design Center at Texas Instruments, on the development of sensors and control in semiconductor processing, and on design studies of thermofluid systems in semiconductor process technology. His group at the Sandia Combustion Research Facility is involved in a range of computational reacting flow research funded by the U.S. Department of Energy, Basic Energy Sciences/Chemical Sciences Division and the DOE SciDAC Computational Chemistry program. This work spans the development of algorithms for time integration and uncertainty quantification, distributed high-performance component software implementations, and computational studies of reacting flow with detailed hydrocarbon kinetics. The group also works on DARPA-funded research focused on detailed modeling and uncertainty quantification in electrochemical microfluid systems. He is coauthor of over 30 archival journal articles and four U.S. patents.